1,2,4-Triazole Complexes XII *

Magnetic properties of Fe (1, 2, 4-triazole)$_2$ (NCS)$_2$, a quasi two-dimensional S = $\frac{1}{2}$. antiferromagnet with hidden canting.

D. W. Engelfriet, W. L. Groeneveld

Department Inorganic Chemistry, Gorlaeus Laboratoria, Rijksuniversiteit, Leiden, The Netherlands

and

G. M. Nap

Kamerlingh Onnes Laboratorium, Rijksuniversiteit, Leiden, The Netherlands

Z. Naturforsch. **35a**, 852–864 (1980); received June 12, 1980

Fe(trz)$_2$(NCS)$_2$ has been investigated by means of magnetic susceptibility and magnetization measurements on single crystals at temperatures 1.8–300 K, heat capacity measurements at 1.5–90 K and neutron powder diffraction at 1.2 K. The compound orders antiferromagnetically at $T_c = 8.46(2)$ K. The susceptibilities along the orthorhombic axes are strongly anisotropic, the a axis being the preferred direction. The susceptibility data along a and the heat capacity results are in reasonable agreement with the predictions for the quadratic layer, $S = \frac{1}{2}$. Ising antiferromagnet, with an intralayer exchange constant $J/k = -7.2(2)$ K. Below T_c the magnetization curve along the a axis reveals a metamagnetic transition at 1.74 kOe. In accordance with the Ising-like properties, a direct transition from the antiferromagnetic to the paramagnetic state is observed along a at 50 kOe.

Hidden canting is found to be present. At 1.2 K the compound appears to be monoclinically distorted with $\alpha = 88.3°$ (with respect to Aba2, the space group at 300 K). The magnetic structure consists probably of four sublattices with the magnetic moments lying in the planes $z = 0$ and $z = \frac{1}{2}$ (with respect to the distorted cell in Aba2) along directions that are at an angle of 8° with the a axis.

Ligand bonding parameters are discussed in terms of the angular overlap model.

Introduction

Previous reports of the present series of papers have shown that 1,2,4-triazole (trz) and its derivatives often yield metal complexes in which these ligands act as bridging groups [1 – 6].

From X-ray single crystal diffraction experiments it was found that the compounds of formula M(II) (trz)$_2$(NCS)$_2$, with M = Co, Zn and Cu, have very similar layered crystal structures [1]. From the X-ray powder diffraction patterns the Mn, Fe, Co and β-Ni members of the series were found to be isomorphous [2]. As may be expected from their crystal structure, these materials exhibit 2-d (d = dimensional) properties. Mn(trz)$_2$(NCS)$_2$ behaves as a 2-d, $S = 5/2$ Heisenberg antiferromagnet [3] and Co(trz)$_2$(NCS)$_2$ as a 2-d, $S = \frac{1}{2}$, XY antiferromagnet with hidden canting [4].

Very recently, it was shown by X-ray single crystal diffraction that the structures of the Fe and Co compounds are practically identical [5]. Also, the results of magnetic measurements on powders are very similar [6]. Susceptibility measurements on powdered Fe(trz)$_2$(NCS)$_2$ revealed a large peak at 8.8 K, and in the magnetization vs. field curve a jump was found at 1.7 kOe. These results were ascribed to the presence of spin canting, possibly related to the tilted FeN_6 octahedra in the crystal structure [5, 6].

In order to obtain a more complete picture of its magnetic properties, Fe(trz)$_2$(NCS)$_2$ has been studied by means of susceptibility and magnetization measurements on single crystals and by heat capacity measurements and neutron diffraction experiments on powders.

Crystal Structure

Fe(trz)$_2$(NCS)$_2$ is orthorhombic, space group Aba2, with $a = 7.882$, $b = 16.312$, $c = 9.890$ Å and $Z = 4$. The structure is depicted in Figure 1. Fe(II)

* Part XI, D. W. Engelfriet and G. C. Verschoor, Acta Cryst. submitted. Requests for reprints should be sent to Drs. D. W. Engelfriet, Gorlaeus Laboratoria, P. O. Box 9502, 2300 RA Leiden, The Netherlands.

0340-4811 / 80 / 0800-0852 $ 01.00/0. — Please order a reprint rather than making your own copy.

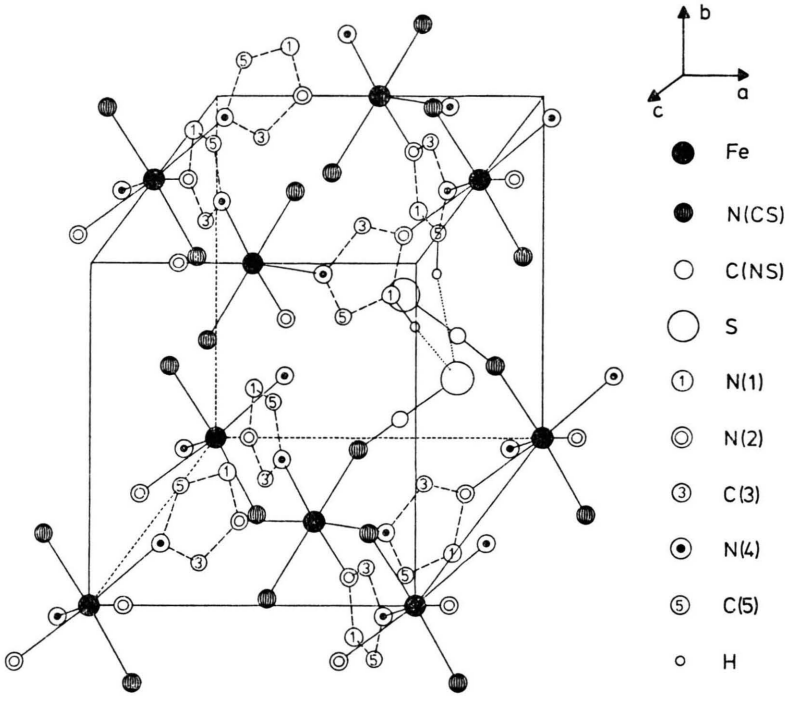

Fig. 1. FIGATOM [7] drawing of the crystal structure of $Fe(trz)_2(NCS)_2$. The top half of the unit cell has been omitted. For clarity only two NCS groups and two H atoms are shown. Possible interlayer hydrogen bonding is indicated by dotted lines.

ions are at special positions (0, 0, 0) and $(0, \frac{1}{2}, \frac{1}{2})$. They are connected by trz groups in the planes $y = 0$ and $y = \frac{1}{2}$, and thus a layered structure is formed. N-donating NCS^- groups protrude on either side of the layers. The FeN_6 octahedra are tilted in the planes $z = 0$ and $z = \frac{1}{2}$, the angle with the b direction being 31°. Exchange interactions between neighbouring Fe ions may take place via the following paths: (a) via the bridging trz groups in the planes $y = 0$ and $y = \frac{1}{2}$, (b) via hydrogen bonding between the sulphur atom of an NCS^- group in one layer and a H(1) atom of a trz group in a neighbouring layer (see Figure 1). The strongest exchange will take place via path (a), so that in the layers the Fe ions are connected *equivalently* to four nearest magnetic neighbours. Hence the planes $y = 0$ and $y = \frac{1}{2}$ can be considered as quasi-quadratic magnetic lattices. From the large number of non-magnetic atoms involved in path (b), one expects the interlayer interactions to be much weaker than the intralayer exchange, resulting in the observed 2-d properties.

Further, it should be mentioned that the trz rings are disordered. In the refinement of the X-ray data it was found that 40% of the trz rings are rotated over 180° around a pseudo two-fold axis pointing from C(3) to the midpoint between N(1) and C(5) [1, 5]. Therefore, effectively, both H(1) and H(5) in the structure as shown in Fig. 1 can be considered to form a hydrogen bond to the NCS^- group. Recent Mössbauer measurements seem to indicate that the trz rings are reversed in a random way throughout the structure [8].

Experimental

Single crystals were prepared in the following way. A solution of $FeCl_2 \cdot 4\,H_2O$, acidified with HCl, was added to a solution containing equimolar quantities of trz and NH_4NCS. The concentration of $Fe(trz)_2(NCS)$ was approximately 0.1 mmol/ml. SO_2 was passed through the solution to reduce Fe(III). A beaker with the solution was placed over P_2O_5 in a dessicator which was flushed with N_2. After 1 – 2 weeks very pale green crystals appeared which were isolated, dried with filter paper and stored over P_2O_5. The crystals are rather flat and diamond-shaped. Often the diamond is elongated to a parallelogram. Like in the Mn and Co compounds, the b axis is perpendicular to the flat surface and the a and c axes are along the bisectors of the diamond or parallelogram. A number of cyrstals with a total

mass of 17.85 mg was mounted with Apiezon grease in a delrin cube which was attached to the sample rod of a commercial vibrating sample magnetometer, equipped with a superconducting magnet supplying fields up to 56 kOe [9]. Measurements at 80 – 300 K were performed with a Faraday balance [10].

All measured susceptibilities and magnetizations were corrected for diamagnetism, using a value of $156(5) \times 10^{-6}$ e.m.u./mole, as was determined for the Zn compound.

Heat capacity measurements were performed at 1.5 – 90 K on a powdered sample, compressed into a calorimeter can, using conventional heat pulse techniques [11].

The neutron diffraction pattern at 1.2 K was recorded using the powder diffractometer at the HFR reactor at Petten.

Results and Discussion

Heat Capacity Measurements

The measured specific heat of $Fe(trz)_2(NCS)_2$ is shown in Figure 2. From the lamda like peak the ordering temperature is found as $T_c = 8.46(2)$ K. To obtain the magnetic heat capacity (C_M), the lattice heat capacity (C_L) has to be subtracted from the experimental data. No temperature region could be found where the lattice and magnetic contributions could be separated by means of the relation $C = C_L + C_M = a\,T^3 + b\,T^{-2}$. However, for the corresponding Cu and Mn compounds the lattice contribution could be determined sufficiently accurate, due to their lower transition temperatures ($T_c =$ 0.7 K and 3.29 K for the Cu and Mn compounds, respectively). Therefore we tried to determine C_L in the Fe compound by scaling the lattice contributions of the Cu and Mn compounds, using the relation [12]

$$C_{L,Fe}(T) = C_{L,M}(T/r) \qquad (1)$$

with M = Cu or Mn. It soon became clear that the Fe ions are in a pseudo doublet ground state with an effective $S = \frac{1}{2}$ and that there are contributions to the specific heat due to higher energy levels. Thus, after subtraction of a trial lattice contribution, the resulting C_M vs. T curve had a total magnetic entropy

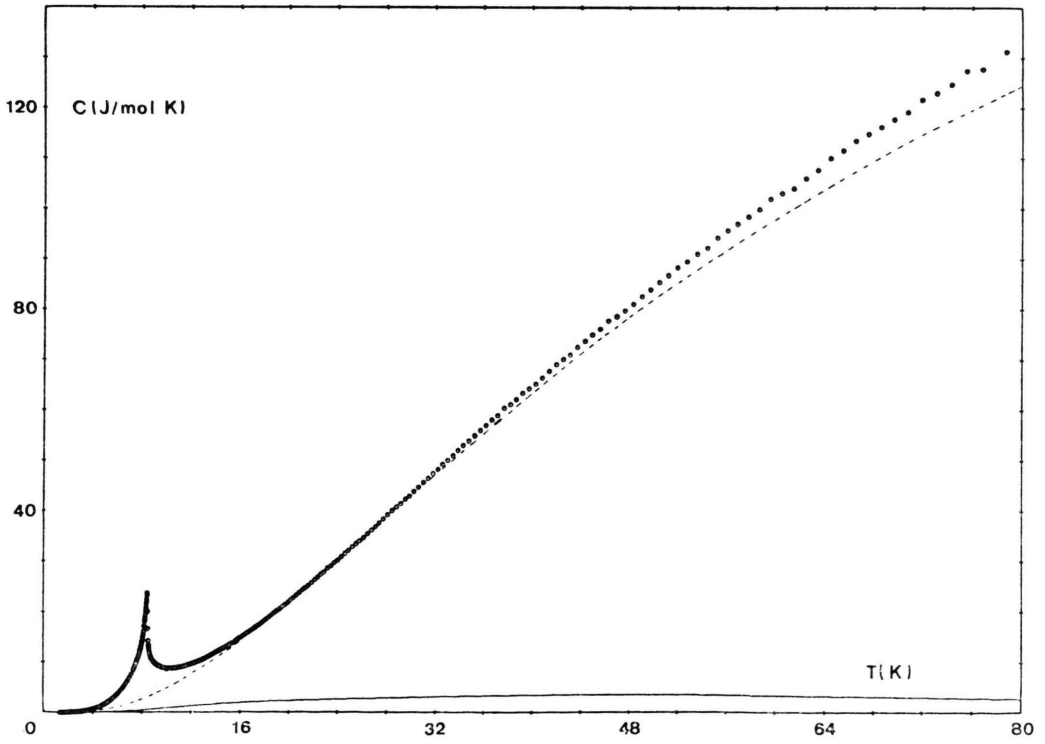

Fig. 2. The heat capacity as a function of temperature. The full line is the Schottky contribution arising from levels at 45, 120 and 150 K above the ground doublet. The dashed line is the sum of the Schottky and lattice contributions.

below 20 K that was close to $R \ln 2 = 5.76$ J/mole K, which is the theoretical value for an $S = \frac{1}{2}$ system. Further conditions are that, of course, $C_M > 0$ and that at higher temperatures $C_M \propto T^{-2}$. It appeared to be impossible to find such a C_M vs. T curve by merely varying r (in Equation (1)). This had to be ascribed to the presence of an energy level relatively close (at ~ 40 K) to the doublet ground state. In order to obtain the positions of the energy levels, the principal susceptibility data at 80 – 300 K (corrected for the presence of exchange) were fitted to angular overlap parameters using the program CAMMAG [13, 14] (see last section). The five lowest levels were found at 0, 3, 66, 90 and 110 K, respectively. In subsequent trials we subtracted from the total specific heat a Schottky contribution, arising from levels at 66, 90 and 110 K above the ground doublet, together with a scaled lattice contribution, trying different values for r in (1). In this way still no acceptable specific heat curve could be obtained, unless the three higher levels were shifted somewhat. This seems justified, as the CAMMAG program does not account for the presence of exchange and because the fit to the susceptibility data was by no means unique. A satisfactory result finally came out by placing the higher levels at 45, 120 and 150 K with $r = 1.04$, using the Cu data. The solid curve in Fig. 2 represents the Schottky contribution and the dashed line the sum of the Schottky and lattice contributions which were subtracted from the total heat capacity. The resulting magnetic specific heat is shown in Fig. 3 in a double logarithmic plot.

Figure 2 clearly shows that, apparently, (1) is no longer valid for $T > 25$ K. A similar result was obtained in $Co(trz)_2(NCS)_2$, where (1) lost its validity for $T > 16$ K [4].

In order to determine the total magnetic entropy S_∞ and energy E_0, the curve in Fig. 3 was extrapolated to $T = \infty$. Contributions below $T = 1.5$ K were negligibly small (less than 1%). We found $S_\infty/R = 0.68(3)$ K, which is indeed close to the theoretical value of 0.693 K. 54% of the entropy is gained below T_c. The total magnetic energy amounts to $E_0/R = 7.2(3)$ K of which 36% is gained below T_c. As can be seen from Fig. 3 the magnetic specific heat fits reasonably well to the predictions for the quadratic $S = \frac{1}{2}$ Ising model [15], with $J/k = -7.2(1)$ K. From the magnetic energy $|J|/k = 7.2(3)$ is calculated by means of the relation

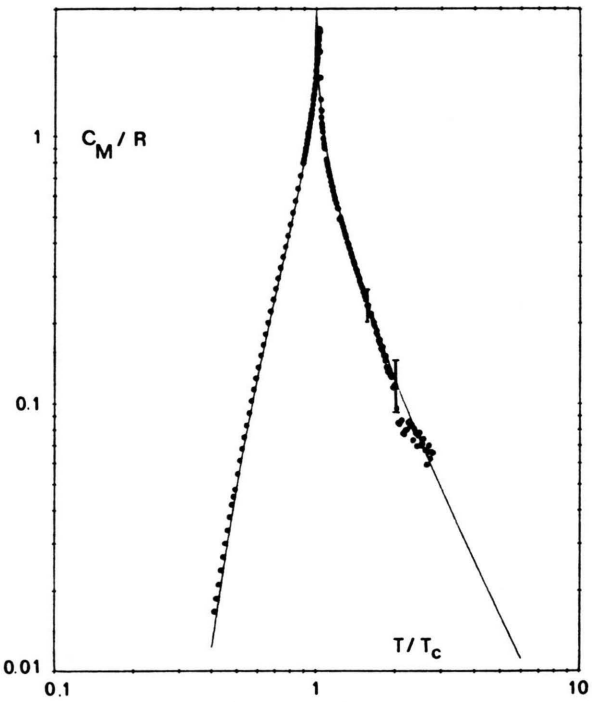

Fig. 3. The magnetic heat capacity compared with the predictions for the Ising, $S = \frac{1}{2}$ quadratic lattice with $J/k = -7.2$ K.

$E_0/R = z\,|J|\,S^2/k$, with $z = 4$ (the number of nearest magnetic neighbours). Close to T_c there are deviations from the ideal 2-d behaviour. The experimental peak does not coincide with the theoretical curve and on the high temperature side the experimental specific heat drops more rapidly than the theoretical curve. Apparently, near T_c the weak interlayer interactions (see below) lead to a crossover from 2-d to 3-d behaviour. These deviations from ideality also show up in the critical values, given in Table 1.

Table 1. Comparison of critical entropy and energy values with theoretical results for Ising lattices with $S = \frac{1}{2}$ ($\theta = 2z\,|J|\,S(S+1)/3k$).

	2-d square lattice ($z = 4$) [15]	$Fe(trz)_2(NCS)_2$ (this work)	simple cubic lattice ($z = 6$) [16]
kT_c/J	1.135	1.18	2.255
T_c/θ	0.567	0.59	0.752
S_c/R	0.306	0.37	0.558
S_c/S_∞	0.442	0.54	0.805
$(S_\infty - S_c)/R$	0.386	0.32	0.135
$-E_c/RT_c$	0.623	0.54	0.220
$(E_c - E_0)/RT_c$	0.258	0.31	0.445

Susceptibility Measurements

Magnetic susceptibilities measured along the *a* and *c* directions at a field of 2.79 kOe are depicted in Figure 4. The broad maximum in the χ_a vs. T curve is another indication of low dimensional magnetic behaviour. The *a*-axis appears to be the preferred direction of antiferromagnetic alignment and the *c* axis is a perpendicular direction.

The maximum in the χ_a vs. T curve occurs at $T = 12.2(2)$ K with $\chi_a(\max) = 0.204(4)$ e.m.u./mole. From the point of maximum slope the transition temperature is estimated as $T_c = 8.5(1)$ K, in agreement with the value obtained from the heat capacity measurements.

Figure 5 shows the magnetization as a function of temperature measured along *b*. Except for the region $8 < T < 10$ K, M_b/H_b is independent of the applied field, which was 0.79 kOe. The sharp peak at 9.0 K indicates the presence of weak ferromagnetic moments due to spin canting. The point of maximum slope yields $T_c \cong 8.7$ K, a somewhat higher value than that obtained from the other experimental results. A much smaller peak is also found along *c*. This peak was observed on several crystals and it is therefore unlikely that it is caused by misorientation, as the shape of the crystals allows an accurate orientation perpendicular to the *b* axis. As will become apparent in the discussion of the neutron diffraction results, this peak can be caused by spin canting too, owing to a small monoclinic distortion below T_c.

On basis of the results from the previous section, the susceptibility data in the *a* direction were compared with the predictions for the parallel susceptibility of the quadratic Ising lattice with $S = \frac{1}{2}$ [17]. For $8 < T < 14$ K a fair fit was obtained with $J/k = -7.2(2)$ K, $g_a = 8.5(1)$ and $\chi_{tip} = 0$ (full line in Figure 4). Below T_c the χ_a data do not extrapolate

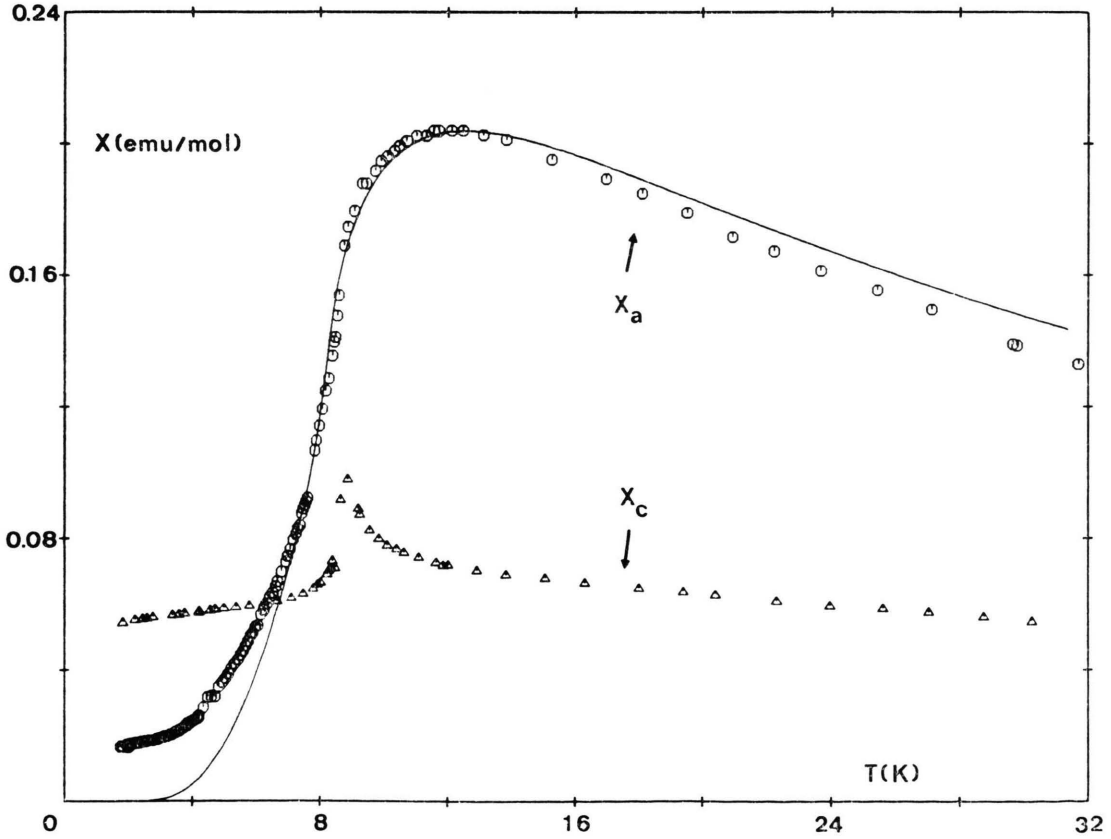

Fig. 4. Magnetic susceptibility as a function of temperature along the *a* and *c* axes measured at $H = 2.79$ kOe. The drawn line is the prediction for the parallel susceptibility of the quadratic, $S = \frac{1}{2}$, Ising antiferromagnet with $J/k = -7.2$ K and $g_a = 8.5$.

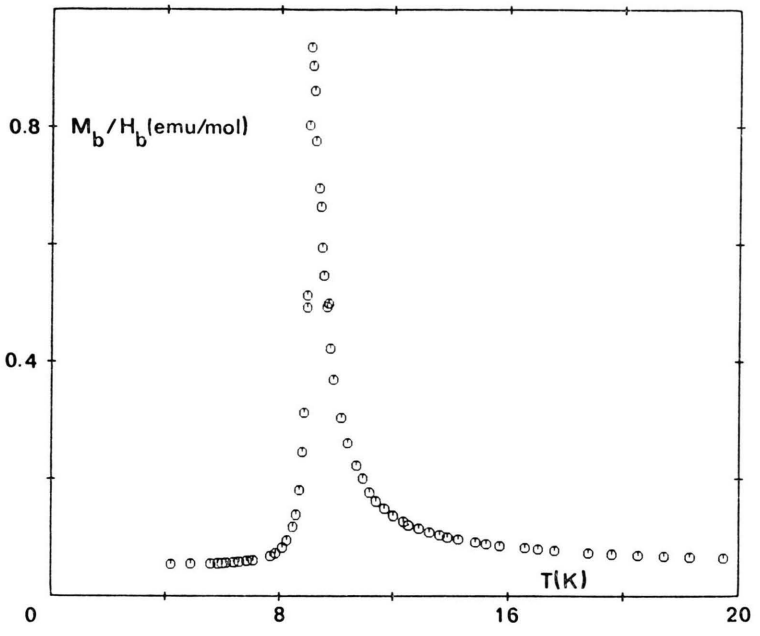

Fig. 5. Magnetization as a function of temperature measured along the *b* axis at $H = 0.79$ kOe.

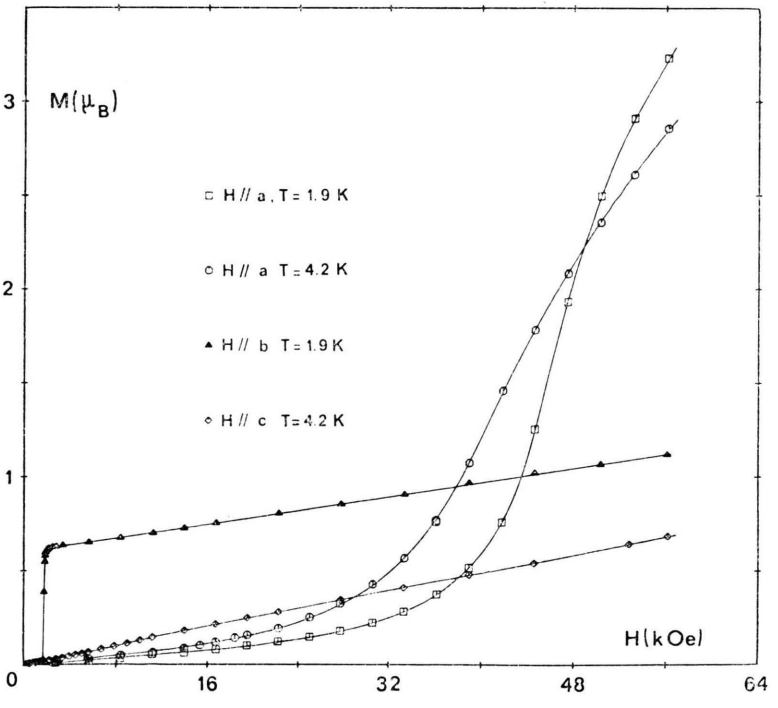

Fig. 6. Magnetization curves measured along the *a*, *b* and *c* directions.

to zero as one would expect for an easy direction. This deviation may, however, be ascribed to a canting of the spins away from the *a* axis (see next section). The discrepancy between theory and experiment for $T > 14$ K is obviously attributable to contributions from higher energy levels relatively close to the ground doublet as we already found in the analysis of the heat capacity data.

Magnetization Measurements

Figure 6 represents the magnetization as a function of the applied field along the three orthorhombic

directions at several temperatures below T_c. At $T = 1.9$ K with $H//a$ the magnetization curve displays a transition at a critical field $H_c{}^a = 48(2)$ kOe (region of maximum slope). At 4.2 K the value of $H_c{}^a$ is approximately 42 kOe. The relatively strong temperature dependence of $H_c{}^a$ and the high value of the magnetization attained at 56 kOe (75% of the saturated moment), suggest that this is not a spin-flop transition, but a direct transition from the antiferromagnetic into the paramagnetic state. The occurrence of such a transition is in accordance with the observed Ising character of the substance [18]. In an Ising antiferromagnet the magnetic moments become ferromagnetically aligned at a critical field, which at $T = 0$ K is given by the molecular field approximation [19]:

$$2z|J|S = g_a \mu_B H_c{}^a(0). \qquad (2)$$

Using an estimated value of 50 kOe for $H_c{}^a(0)$ and $g_a = 8.5$, (2) yields $|J|/k = 7.1$ K, which agrees very well with the values found from the susceptibility and heat capacity measurements.

Next we turn to the magnetization measurements with $H//b$. At temperatures well below T_c the magnetization increases slowly up to a critical field of 1.4 kOe, where it rises steeply to 0.63 μ_B (Figure 7). From 1.5 to 56 kOe the magnetization increases almost linearly (Figure 6). The value of the critical field $H_c{}^b$ is taken as the point of maximum slope in the M_b vs. H curve. As Fig. 7 demonstrates, the magnitude of the jump in M_b and the values of $H_c{}^b$ both decrease with increasing temperature. Figure 8 gives the magnetic phase diagram. The points are remarkably close to the dashed line, which represents data from the isomorphous Co compound, which exhibits a similar transition along its a axis [4]. This type of transition is usually called metamagnetic [20]. The M_c vs. H curve at 4.2 K is almost a straight line, apart from a small change in slope near $H \cong 7$ kOe. This slight departure from linearity, which is hardly visible on the scale of Fig. 6, will be caused by the already mentioned monoclinic distortion.

The magnetizations along b and c at higher field strength will mainly be due to contributions from higher energy levels by the second order Zeeman effect. From the slope of the linear part of the magnetization curves above 25 kOe these contributions are estimated as $\chi_{b,\mathrm{tip}} \cong 0.04$ and $\chi_{c,\mathrm{tip}} \cong 0.05$ e.m.u./mole. By subtracting these values from the measured susceptibilities along b and c we obtain $g_b \cong 2.0$ and $g_c \cong 1.5$. Thus g_b, $g_c \ll g_a$ ($= 8.5$), which is to be expected in the case of Ising-like behaviour.

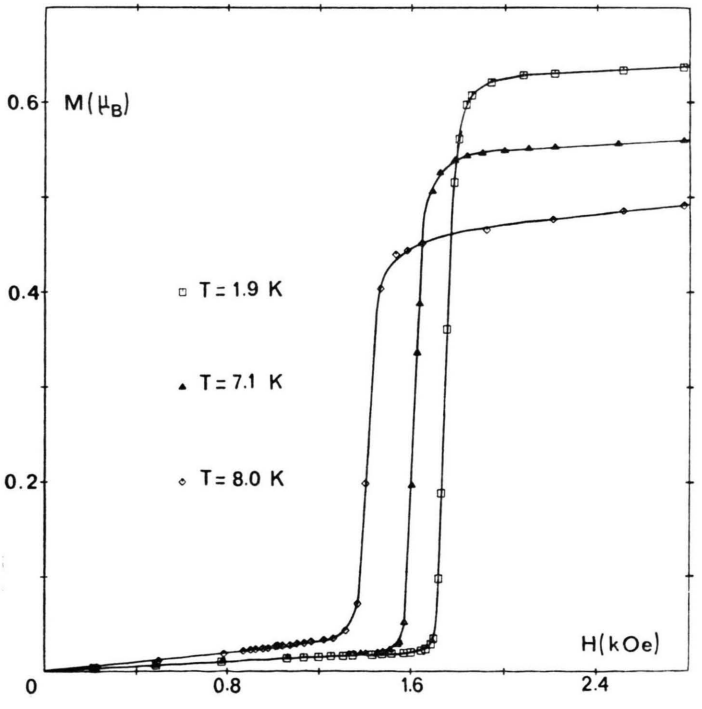

Fig. 7. Magnetization curves measured along b at different temperatures.

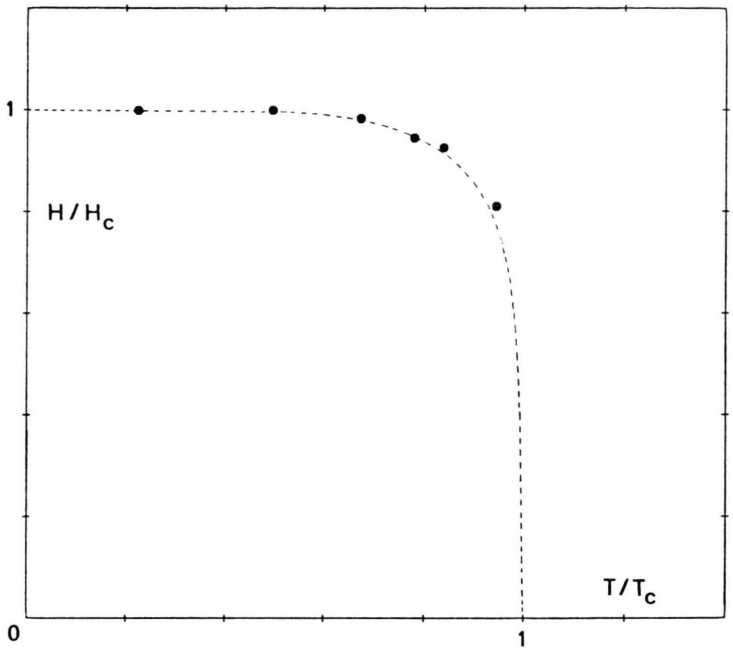

Fig. 8. Temperature dependence of the critical field H_c^b as obtained from M_b vs H measurements, in reduced units ($H_c^b(0) = 1.74$ kOe, $T_c = 8.46$ K). The dashed line represents data obtained along the a direction in $Co(trz)_2(NCS)_2$ ($H_c^a(0) = 1.015$ kOe, $T_c = 5.72$ K).

Magnetic Structure and Interlayer Interactions

The peaked M_b vs. T curve can be explained by the existence of weak ferromagnetic moments parallel to b, owing to spin canting. The peak is caused by hidden canting, since the magnetization measurements reveal that there is no net moment in low fields. From this conclusion, together with the observations that the a axis is nearly an easy direction and that only minor anomalies occur along c, we deduce that the magnetic moments are canted away from the a direction and are lying almost perpendicular to the c direction. Thus the magnetic structure probably consists of four sublattices, as shown in Figure 9 a. M_1 and M_2 belong to one layer and M_3 and M_4 to a neighbouring one. Because of the canting, the layers possess net moments (along b), which are antiparallel in adjacent layers. The jump in the M_b vs. H curves can now be explained by assuming that at the critical field H_c^b all net moments of the layers become aligned in the b direction. This implies a reversal of the directions of half of the spins (Figure 9 b). Similarly, at the critical field H_c^a, the a-components of the magnetic moments become aligned along a. This transition will result in a arrangement as shown in Figure 9 c.

The canting angle γ of the magnetic moments with respect to the a axis can be calculated from the jump ΔM in the M_b vs. H curve by means of the relation:

$$\operatorname{tg}\gamma = \Delta M / M_s . \tag{3}$$

With $\Delta M = 0.63(3)\ \mu_B$ (from Fig. 7), taking the saturation magnetization along a as $M_s = \frac{1}{2} g_a \mu_B = 4.25(10)\,\mu_B$, (3) yields $\gamma = 8.4(5)^\circ$.

The interlayer exchange coupling can be calculated from the values of H_c^b and ΔM. The interlayer exchange energy is given by $-z' \mid J' \mid S^2$, where z' is the number of nearest magnetic neighbours of an Fe

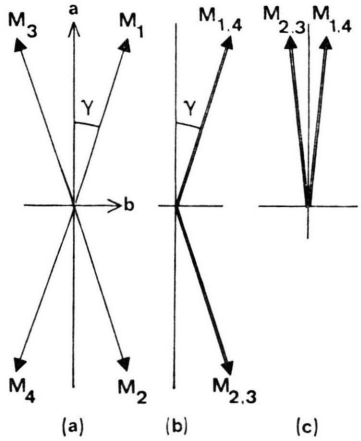

Fig. 9. The four sublattices in the magnetic structures at $H = 0\,(a)$, $H^b > H_c^b\,(b)$, and $H^a > H_c^a\,(c)$.

ion in adjacent layers and J' is the interlayer exchange coupling parameter. From Fig. 1 it can be inferred that z' may be as much as eight. At the transition the changes in Zeeman energy and the interlayer exchange energy should be equal so that (at $T = 0$ K) we have:

$$2z' \mid J' \mid S^2 = H_c{}^b \Delta M . \qquad (4)$$

By substituting $\Delta M = 0.63(3)\mu_B$ and $H_c{}^b = 1.74(1)$ kOe, we calculate $z' \mid J' \mid /k = 0.15(1)$ K and $z' \mid J' \mid S^2/k = 3.7(2) \times 10^{-2}$ K. The ratio of inter- to intralayer exchange thus becomes $z' \mid J' \mid /z \mid J \mid = 5.2(4) \times 10^{-3}$.

Neutron Diffraction

From the arguments presented in the discussion of the neutron diffraction results for the Mn and Co compounds [3, 4] and the observation that the a axis is the preferred direction, the magnetic space group for $Fe(trz)_2(NCS)_2$ might be $A_Pba'2'$. In that case we should have $M_x > M_y$ and $M_z = 0$. To verify this the compound was investigated by neutron powder diffraction below T_c. The diffraction pattern show in Fig. 10 was recorded at 1.2 K in the range $5.4° < 2\theta < 75°$. The neutron wave length was 2.5855 Å. The peak-to-background ratio is poor, owing to the high hydrogen content. The diagram clearly shows reflections indexed as 001 and 021 which are forbidden in Aba2, indicating that the magnetic lattice will be primitive.

The data were analysed by means of Rietveld's profile program [21]. Atomic form factors for Fe(II) were taken from Watson and Freeman [22] and scattering lengths from Bacon [23]. The agreement indices which are referred to have been given previously [4, 21]. The profile intensities (y_i) were corrected for preferred orientation according to $y_i(\text{corr}) = y_i(\text{obs}) \exp(-G\alpha^2)$.

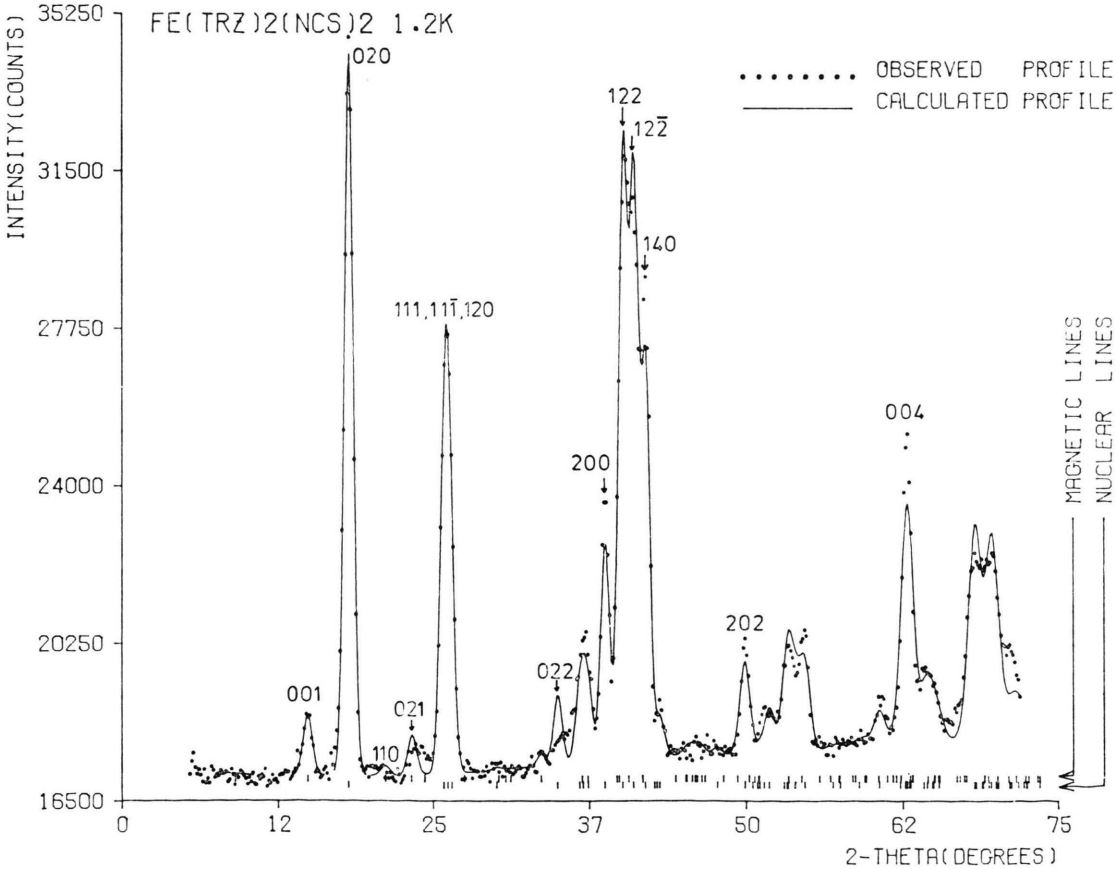

Fig. 10. Neutron diffraction pattern at 1.2 K. Only some reflections have been labelled.

α is the acute angle between the scattering vector and the normal of the platelike crystallites. G is called the preferred orientation parameter. The structural parameters used in the refinement were those found by X-ray diffraction at room temperature and were kept constant. Refinement in $A_pba'2'$ turned out to be impossible. Certain nuclear reflections appear to be broadened, e. g. the reflection 122 (in Aba2). This reflection is split up in two reflections which we tentatively indexed as 122 and $12\bar{2}$. This implies that the cell becomes monoclinic with $\alpha + 90°$ (with respect to Aba2). In that case the space group could be Ab. A more regular setting would be Pn, which can be obtained by means of the transformation

$$\begin{pmatrix} a' \\ b' \\ c' \end{pmatrix} = \begin{pmatrix} 0 & \frac{1}{2} & \frac{1}{2} \\ 1 & 0 & 0 \\ 0 & \frac{1}{2} & -\frac{1}{2} \end{pmatrix} \begin{pmatrix} a \\ b \\ c \end{pmatrix}$$

with $b' (\equiv c)$ as the monoclinic axis.

It is interesting to mention that the Cu compound of the series is in the same way monoclinically distorted [1]. A satisfactory result with $\alpha = 88.27(2)°$ was obtained after several cycles of refinement, keeping the components of the magnetic moments fixed at the values $M_x = 4.3\ \mu_B$, $M_y = 0.65\ \mu_B$ and $M_z = 0$ which were found from the magnetization measurements. Refinement of M_x and M_y resulted in $M_x = 4.1\ \mu_B$ and $M_y = 1.2\ \mu_B$. The latter value should be regarded as unrealistic when compared with the magnetization results. It must be pointed out, however, that M_y is calculated from the intensities of relatively weak magnetic reflections, many of which are obscured by overlapping nuclear reflections. The value of M_y will therefore be very sensitive to changes in the positional parameters (which were not refined) and to small variations in the estimated background intensity. The same will be true for M_z which may be non-zero due to the lower symmetry. However, comparison of the peaks in the χ_b and χ_c curves suggests that $M_z \ll M_y$. Therefore we kept $M_z = 0$ and $M_y/M_x = 0.65/4.3$ in the final least-squares cycles. The fit thus obtained is represented by the drawn line in Figure 10. Some relevant parameters are listed in Table 2.

Although Fig. 10 shows that not all reflection intensities have been adequately accounted for, there is good agreement between calculated and observed peak positions. In view of the limited accuracy of the data, we have refrained from further improvements like refinement of positional parameters.

Table 2. Neutron diffraction results at 1.2 K. 1 σ standard deviations as calculated by the least-squares program are given in parentheses. For comparison the axes at room temperature have been included.

$T = 300$ K, Aba2;	$a = 7.882\ (1)$ Å;	$b = 16.312\ (4)$ Å;
	$c = 9.890\ (2)$ Å	
(X-ray single crystal diffraction).		
$T = 1.2$ K, Apb(?)	$a = 7.776\ (3)$ Å;	$b = 16.258\ (8)$ Å;
	$c = 9.914\ (4)$ Å;	$\alpha = 88.27\ (2)°$
(Neutron powder diffraction).		
$M_x = 4.2\ (2)\ \mu_B$;	$M_y = 0.64\ \mu_B$;	$M_z \cong 0$;
$R_{nucl.} = 5.4\%$;	$R_{magn.} = 21.4\%$;	$\chi^2 = 8.0$;
		$G = 0.118$.

Because the transition temperature to the monoclinic phase is not known, no reference was made to the monoclinic axes in the previous sections.

The magnetic moments are expected to be arranged as sketched in Fig. 11 which is essentially the magnetic structure in $A_pba'2'$, with $\alpha + 90°$. Because the small peak in the χ_c curve indicates that the weakly ferromagnetic moments of the layers have a small component in the c direction, the magnetic moments shown in Fig. 11 are probably perpendicular to c^*.

Canting Mechanism

The magnetization measurements reveal that the magnetic moments are at angles of $+8.4°$ and $-8.4°$ with the a axis. This situation is analogous to that encountered in $Co(trz)_2(NCS)_2$ [4], where it was found that the magnetic moments are at angles of $7.4°$ and $-7.4°$ with the b direction. Further-

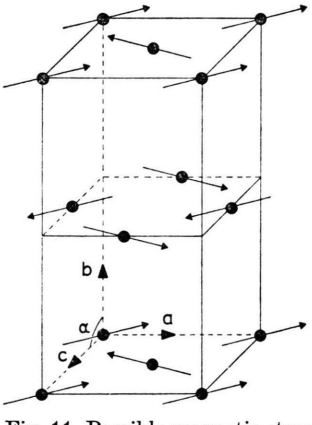

Fig. 11. Possible magnetic structure of $Fe(trz)_2(NCS)_2$. The magnetic moments are perpendicular to c^*.

more, ESR measurements on the Co-doped Zn compound (which is nearly isostructural [1]) indicated the presence of two inequivalent sites whose anisotropic g-tensors are tilted in the $a-b$ plane, making angles of $+10^\circ$ and -10° with the b direction. Hence, the most appropriate canting mechanism was considered to be the one given by Silvera et al. [24], who showed that anisotropic g-tensors that are mutually tilted can give rise to large canting angles. In view of the many similarities between the Co and Fe compounds, it can be assumed that this mechanism is present in both compounds. A quantitative comparison with Silvera's model, which yielded satisfactory results in $Co(trz)_2(NCS)_2$ is not possible here, as the values of g_b and g_c could not be determined accurately. Because the canting angles of the magnetic moments do not differ very much, the canting angle of the g-tensors in $Fe(trz)_2(NCS)_2$ will be close to 10° also.

We shall now calculate the value of the isotropic intralayer exchange parameter [25], which is needed in the following section. The real spin S can be expressed into the effective spin S according to

$$S_i = \tfrac{1}{2}\, g_i^s\, s_i \qquad (5)$$

where $i = x', y', z'$ refer to the principal axes of the tilted g-tensors. Ignoring the small monoclinic distortion, we suppose that y' coincides with the c direction and that the z' directions are at angles $\vartheta = +10^\circ$ and -10° with the a axis. Further, the magnetic interaction between the true spin moments is considered to be isotropic:

$$H_{\text{int}} = -2\tilde{J} \sum_{j,k} S_j S_k .$$

Rewriting in terms of the spin components with respect to the local g-tensor axes [24] yields:

$$\begin{aligned} H_{\text{int}} = -2\tilde{J} \sum_{j,k} [&\cos 2\vartheta\, S_{jx'} S_{kx'} + S_{jy'} S_{ky'} \\ &+ \cos 2\vartheta\, S_{jz'} S_{kz'} \\ &+ \sin 2\vartheta\, (S_{jx'} S_{kz'} - S_{jz'} S_{kx'})] . \end{aligned} \qquad (6)$$

As the magnetic behaviour of $Fe(trz)_2(NCS)_2$ is Ising-like at sufficiently low temperatures, we conclude that the effective interaction hamiltonian

$$H_{\text{eff}} = -2J \sum_{j,k} s_{jz'} s_{kz'} \qquad (7)$$

will be closely approximated (the term $\cos 2\vartheta$ which should occur in Eq. (7) has been included in J).

From (5), (6) (7) it follows that if $g_{z'} \gg g_{x'}$, $g_{y'} \cong 0$:

$$J = 4\tilde{J}/(g_{z'}^s)^2 \cos 2\vartheta . \qquad (8)$$

With the estimate $g_{z'}^s \lesssim 8$, $\vartheta = 10^\circ$ and $J/k = 7.2$ K, (8) yields $\tilde{J}/k \cong 0.5$ K.

Bonding Parameters

As already mentioned in the discussion of the heat capacity measurements the susceptibility data at $80-300$ K were fitted by means of the program CAMMAG [13, 14]. CAMMAG is a system of programs for the calculation and fitting of magnetic susceptibilities, ESR g values and electronic spectra for d^n or f^n configurations. The essence of the method employed in these programs is the use of the angular overlap model (AOM) [26] for the parameterization of the ligand field in terms of local metal-ligand interactions. A review demonstrating the relevance of this method has been published recently [27]. Because the program has been developed for magnetic monomers the magnetic susceptibilities had to be corrected for the presence of magnetic exchange interactions by means of a molecular field (MF) approximation. In the MF model the susceptibility at high temperature is given by $\chi = C/(T-\Theta)$, $\Theta = 2zJS(S+1)/3k$. We will assume that for $80 < T < 300$ K the exchange interaction can be described by the isotropic hamiltonian of Eq. (6) with $S = 2$ and that in the absence of exchange interaction one would have $\chi_{i'} = C_i(T)/T\,(i = a, b, c)$ for the three orthorhombic directions. The Curie "constant" will be temperature dependent due to levels at energies $\sim kT$. The susceptibilities for the three orthorhombic directions can then be written as:

$$\chi_i = \chi_i' T/(T-\Theta) \quad (i = a, b, c) \qquad (9)$$

from which the "monomeric" susceptibilities $\chi_{i'}$ can be calculated. With $\tilde{J}/k \cong 0.5$ K we find $\Theta \cong 8$ K. Although (9) should be regarded as a crude approximation, the order of magnitude of the correction term $T/(T-\Theta)$ seems to be acceptable. Since the differences between the χ_i' values calculated with the aid of (9) and those calculated by the CAMMAG program amount to $\sim 7\%$ at some temperatures, a more sophisticated approach would not make sense.

The AOM calculations were performed within the ^5D basis and the parameter set comprised λ (spin-orbit coupling), k (reduction factor for the orbital moment) and e_σ, $e_{\pi\perp}$, $e_{\pi\|}$ for the coordinating N(2), N(4) and N(CS) atoms. The e_σ and e_π parameters denote the energy shifts of metal $d_{x^2-y^2}$, d_{z^2} and d_{xy}, d_{yz}, d_{xz} orbitals, respectively,

due to metal-ligand interaction. The parameters $e_{\pi\perp}$ and $e_{\pi||}$ refer to π-bonding perpendicular and parallel, respectively, to the ligand planes. In the fitting procedure combinations of the above-mentioned parameters were varied, examining their influence on the principal susceptibilities and the energy levels. To find suitable starting values we used results obtained previously with the AOM model (see [27] and references therein). The main conclusions can be summarized as follows:

1. The e_σ parameters could not be determined sensitively. With $e_\sigma(\mathrm{NCS}) \cong 3500\ \mathrm{cm}^{-1}$ and $e_\sigma(\mathrm{N2, N4}) \cong 4000\ \mathrm{cm}^{-1}$ the positions of the highest energy levels were in fair agreement with the UVV reflectance spectrum.
2. For the NCS group $e_{\pi\perp} = e_{\pi||} = e_{\pi\mathrm{av}} \cong 400\ \mathrm{cm}^{-1}$ was found.
3. No significant metal-ligand interaction was found in the plane of each trz group, hence, $e_{\pi||}(\mathrm{N2}) = e_{\pi||}(\mathrm{N4}) \cong 0$.
4. Perpendicular to the trz planes a substantial amount of π interaction was determined: $e_{\pi\perp}(\mathrm{N2, N4}) \cong 600\ \mathrm{cm}^{-1}$. Although the e_σ and $e_{\pi\perp}$ parameters for the N(2) and N(4) atoms did not seem to differ significantly, a slightly better fit was obtained with either
$$e_\sigma(\mathrm{N2}), e_{\pi\perp}(\mathrm{N2}) \lesssim e_\sigma(\mathrm{N4}), e_{\pi\perp}(\mathrm{N4})$$
or
$$e_\sigma(\mathrm{N4}), e_{\pi\perp}(\mathrm{N4}) \lesssim e_\sigma(\mathrm{N2}), e_{\pi\perp}(\mathrm{N2}).$$
Because $\mathrm{Fe-N(2)} = 2.24$ Å and $\mathrm{Fe-N(4)} = 2.15$ Å [5], the parameters for N(2) were taken to be smaller ones.

In Fig. 12 the (smoothed) experimental susceptibilities, corrected according to (9) are compared with the calculated susceptibilities for the values $e_\sigma(\mathrm{NCS}) = 3700$, $e_{\pi\mathrm{av}}(\mathrm{NCS}) = 400$, $e_\sigma(\mathrm{N2}) = 4200$, $e_{\pi\perp}(\mathrm{N2}) = 610$, $e_\sigma(\mathrm{N4}) = 4600$, $e_{\pi\perp}(\mathrm{N4}) = 670$ (all in cm^{-1}), $k = 1.0$ and $\lambda = -100\ \mathrm{cm}^{-1}$.

No unique fit could be obtained, as variations up to 10% in some parameters produced fits as fair as the one shown in Figure 12. We believe that to some extent this will be caused by ill-defined FeN_6 octahedra, owing to the disordered trz groups. Nevertheless, the above values can be considered as good estimates for the ligand bonding parameters in this compound.

Conclusions

$Fe(trz)_2(NCS)_2$ shows 2-d properties, both structurally and magnetically. The magnetic behaviour can be reasonably well described by predictions for the quadratic layer, $S = \frac{1}{2}$, Ising antiferromagnet, with an intralayer exchange constant $J/k = -7.2(2)$ K. The magnetization measurements indicate hidden canting to be present, and can be explained in terms of a four-sublattice, compensated antiferromagnet. From the metamagnetic transition occurring along b it is deduced that the canting angle of the magnetic moments is 8°, away from the a direction. The canting is attributable to tilting of the anisotropic g-tensors in the $a-b$ plane. The Ising-like properties explain the occurrence of a transition along a from the antiferromagnetic into

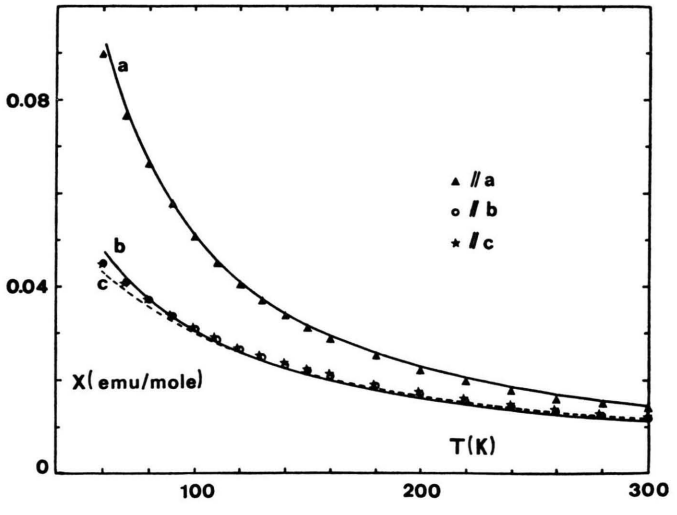

Fig. 12. High-temperature susceptibilities, corrected for the presence of exchange. The drawn curves represent the fit described in the text.

the paramagnetic state at ca. 50 kOe. The ratio of inter- to intralayer exchange $|z'J'|/|zJ|$ is found to be only 5.2×10^{-3}, which explains the observed 2-*d* character. The interlayer interactions will be responsible for the deviations from the ideal 2-*d* behaviour observed in the specific heat curve. A fit of the high-temperature susceptibility data by means of the angular overlap model yields rather unexceptional values for the ligand bonding parameters. The trz groups are found to act as moderately strong π donors.

Acknowledgements

The authors wish to thank Mr. J. F. Strang of the ECN at Petten for recording the neutron diffraction data, Dr. L. J. de Jongh and Prof. Dr. J. Reedijk for discussions and a critical reading of the manuscript and Dr. R. B. Helmholdt for his comments on the neutron diffraction section. One of us (D. W. E.) expresses his gratitude to Dr. M. Gerloch and his group for the hospitality received during a short stay at Cambridge.

[1] D. W. Engelfriet, W. den Brinker, G. C. Verschoor, and S. Gorter, Acta Cryst. **B35**, 2922 (1979).
[2] J. G. Haasnoot and W. L. Groeneveld, Z. Naturforsch. **32b**, 553 (1977).
[3] D. W. Engelfriet and W. L. Groeneveld, Z. Naturforsch. **33a**, 848 (1978).
[4] D. W. Engelfriet, W. L. Groeneveld, H. A. Groenendijk, J. J. Smit, and G. M. Nap, Z. Naturforsch. **35a**, 115 (1980).
[5] D. W. Engelfriet and G. C. Verschoor, Acta Cryst. submitted.
[6] D. W. Engelfriet, J. G. Haasnoot, and W. L. Groeneveld, Z. Naturforsch. **32a**, 783 (1977).
[7] G. A. Langlet, J. Appl. Cryst. **5**, 66 (1972).
[8] H. Th. Lefever, R. C. Thiel, and D. W. Engelfriet, in preparation.
[9] H. T. Witteveen, Thesis, Leiden 1973.
[10] J. W. Arbouw, Thesis, Leiden 1974.
[11] F. W. Klaaijsen, Thesis, Leiden 1974.
[12] J. W. Stout and E. Catalano, J. Chem. Phys. **23**, 2013 (1955).
[13] "CAMMAG", FORTRAN program by D. A. Cruse, J. E. Davies, J. H. Harding, M. Gerloch, D. J. Mackay, and R. F. McMeeking.
[14] M. Gerloch and R. F. McMeeking J. Chem. Soc. Dalton Trans. **1975**, 2443.
[15] L. Onsager, Phys. Rev. **65**, 117 (1944).
[16] C. Domb and A. R. Miedema, Prog. Low Temp. Phys. **4**, 296 (1964).
[17] M. F. Sykes and M. E. Fisher, Physica **28**, 919 (1962).
[18] M. E. Fisher, Proc. R. Soc. A **254**, 66 (1960).
[19] L. J. de Jongh and A. R. Miedema, Adv. Phys. **23**, 1 (1974)
[20] E. Stryjewski and N. Giordano, Adv. Phys. **26**, 487 (1977).
[21] H. M. Rietveld, J. Appl. Cryst. **2**, 65 (1969).
[22] R. E. Watson and A. J. Freeman, Acta Cryst. **14**, 27 (1961).
[23] G. E. Bacon, Compilation 1977.
[24] I. F. Silvera, J. H. M. Thornley, and M. Tinkham, Phys. Rev. **136**, A695 (1964).
[25] H. A. Algra, J. Bartholomé, L. J. de Jongh, R. L. Carlin, and J. Reedijk, Physica **93B**, 114 (1978).
[26] C. E. Schäffer, Struct. Bonding **5**, 68 (1968).
[27] M. Gerloch, Prog. Inorg. Chem. **26**, 1 (1979).